PAPER • OPEN ACCESS

Thermal and electrical conductivity of single crystalline kesterite Cu_2ZnSnS_4

View the article online for updates and enhancements.

Materials Research Express

Thermal and electrical conductivity of single crystalline kesterite Cu$_2$ZnSnS$_4$

M Handwerg[1,2,*] , R Mitdank[1], S Levcenco[2], S Schorr[2,3] and S F Fischer[1,*]

1. AG Neue Materialien, Humboldt-Universität zu Berlin, Institut für Physik, Newtonstrasse 15, 12489 Berlin, Germany
2. Helmholtz-Zentrum Berlin für Materialien und Energie GmbH, Hahn-Meitner-Platz 1, 14109 Berlin, Germany
3. Freie Universität Berlin, 12249 Berlin, Germany
* Authors to whom any correspondence should be addressed.

E-mail: handwerg@physik.hu-berlin.de and saskia.fischer@physik.hu-berlin.de

Abstract

For single crystalline sulfur-based kesterite Cu$_2$ZnSnS$_4$ the electrical and thermal conductivity are measured from 20 K to 320 K. The electrical conductivity decreases exponentially with decreasing temperature. The temperature dependence can be assigned to Mott-variable-range-hopping, an electrical transport process within an impurity band in the band gap. With the 3ω-method a thermal conductivity room temperature value of 5.1 $\pm$ 0.5 Wm^{-1}K^{-1} and a maximal value of 8.0 $\pm$ 0.5 Wm^{-1}K^{-1} at 100 K are found. Phonon-phonon-umklapp-scattering can explain the high temperature range from 100 K to 320 K. The low temperature values of the thermal conductivity are dominated by the temperature-dependence of the specific heat capacity, due to a reduced phonon-mean-free-path, owing to phonon-impurity-scattering.

1. Introduction

Inorganic thin film solar cell materials are of high interest to increase the efficiency while decreasing the overall material quantity. Best efficiency values are obtained by CuIn$_x$Ga$_{x-2}$Se$_2$ [1], but due to the rare Indium and Gallium components, these compounds are not favored for terawatt scale application. With a replacement of Indium and Gallium with the non-toxic earth abundant Zinc and Tin and changing the selenium with sulfur, an alternative solar cell absorber can be produced. The Cu$_2$ZnSnS$_4$ (CZTS) and Cu$_2$ZnSnSe$_4$ (CZTSe) materials with their unique crystal structure are called kesterites [2]. Recently it was shown that CZTS crystallizes in the kesterite-type structure as it was shown by results of Rietveld analysis of neutron powder diffraction data [3]. The band gap fulfills the Shockley–Queisser-conditions [4] for a maximized efficiency reaching 12.6% [5] to date. Because of the temperature-dependence of the efficiency for application in solar technology the thermal properties are of interest. Thermal conductivity room temperature values of kesterite crystals are measured by Liu *et al* [6] with values between 3 Wm^{-1}K^{-1} and 5 Wm^{-1}K^{-1}. Polycrystalline values were given by Thompson *et al* (4 Wm^{-1}K^{-1}) [7] and Yang *et al* (3 Wm^{-1}K^{-1}) [8]. However, single crystalline kesterite thermal conductivity values below room temperature remain to be investigated. With the efficiency of solar cell modules varying with temperature, especially in harsh environments thermal management will become an issue and the thermal conductivity data has to be available.

Here, we investigate the thermal conductivity of a kesterite Cu$_2$ZnSnS$_4$ single crystal in the temperature range from 20 K to 320 K. Therefore, we use the electrical 3ω-method, that consists of electrical heater lines which acts simultaneously as heater and as sensor to measure temperature oscillations within the crystal. From the temperature-dependence of the thermal conductivity the influence of multiple scattering events of the phonons is determined. At lower temperatures the scattering of phonons at defects dominates the thermal transport and at higher temperatures the phonon-phonon-Umklapp-scattering has the highest impact.
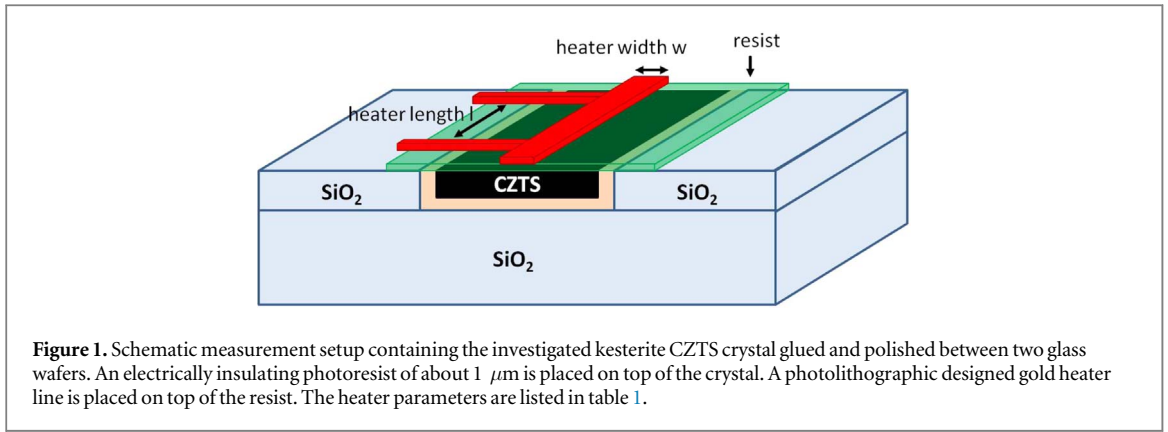
Figure 1. Schematic measurement setup containing the investigated kesterite CZTS crystal glued and polished between two glass wafers. An electrically insulating photoresist of about 1 μm is placed on top of the crystal. A photolithographic designed gold heater line is placed on top of the resist. The heater parameters are listed in table 1.

2. Experimental details

The investigated crystals were grown by chemical vapor transport (CVT) technique using iodine trichloride as a transport agent and powder compound as a starting material. The powder compound has been preliminarily grown in a quartz ampoule by the solid state sintering method using the copper (4N), zinc (4N), and tin (4N) elements and sulphur (4N) element with 5% in excess. After evacuation of the ampoule, it was placed into a vertical single zone furnace. The temperature of the furnace was elevated to about 650 °C with a rate of $\approx$100 °Ch^{-1} and then kept at this level for 30 days to bring the reaction between the sulfur vapors and metals to completion. The polycrystalline starting materials produced by the above-described procedure were used to grow single crystals by the CVT method. The single crystals were grown in a three-zone horizontal gradient furnace with the charge zone maintained at 780 °C and the growth zone at 710 °C. A more detailed information of the growth process is provided in the reference [9]. The structural study and detailed polarized Raman characterization on CZTS kesterite crystal samples have been earlier reported in [9] and in [10]. The crystal of several hundred microns height and width and few millimeters length was glued on a glass substrate. On both sides of the crystal additional glass substrates were placed. Both the glass and the crystal were polished with optical pitch to get a smooth continuous surface. With optical laser lithography two gold line heaters were placed on the polished surface of the crystal. To prevent parallel conduction through the conductive sample, a small ($\approx$1μm) insulating photo resist layer is placed between heater and sample. A measurement setup scheme is pictured in figure 1.

3. Measurement method

The 3ω-method by Cahill [11] is based on the electrical line heater method. Here, a heater line provides a temperature increase with joule-heating and acts simultaneously as sensor which measures *in situ* the temperature. By heating with an alternating current, the temperature oscillation in the heater line follows from the ratio of the first and the third harmonic of the voltage $U_{1\omega}$ and $U_{3\omega}$:
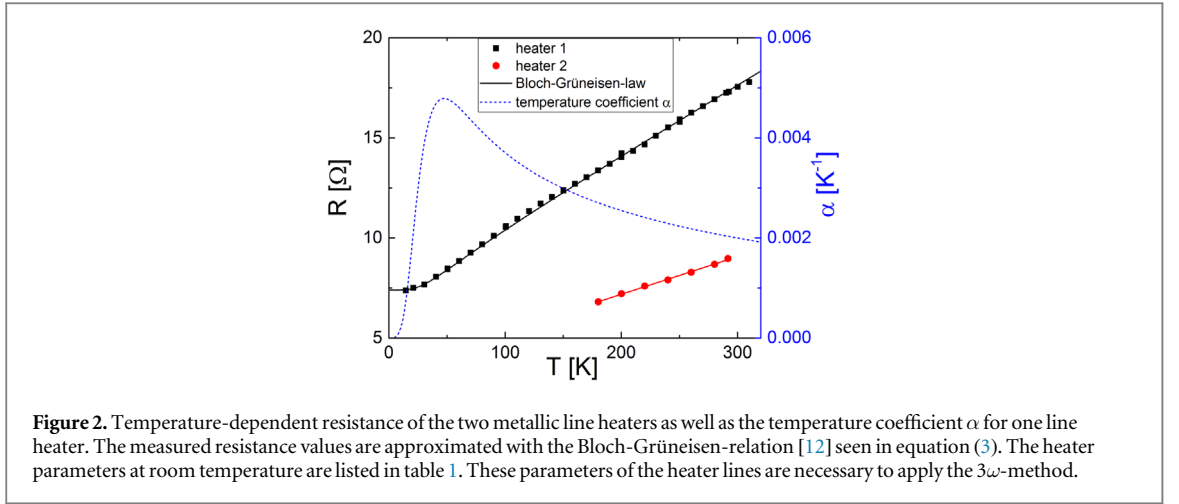
$$\Delta T = \frac{2}{\alpha}\frac{U_{3\omega}}{U_{1\omega}} \tag{1}$$

where $\alpha = (1/R_0) \cdot \partial R/\partial T$ is the temperature coefficient of the heater, R the resistance of the heater and $U_{1\omega}$ the first and $U_{3\omega}$ the third harmonic voltage measured within the heater. Being able to generate heating power P per unit length l of the heater P/l and have a direct relation to the temperature change within the heater, one can calculate the heat which is transported away from the heater line through the substrate. The thermal transport is frequency dependent and the thermal conductivity of the substrate can be obtained best from the linear slope $\Delta T(\ln(2\omega))$ with $\omega = 2\pi f$ as angular frequency. The frequency dependence of the temperature oscillations of the heater is

$$\Delta T \propto \frac{P}{2\pi l\lambda}\ln(2\omega) \tag{2}$$

with λ as thermal conductivity. The frequency dependent 3ω-voltage was measured with a Lock-In-Amplifier SR830.

Before measuring the thermal conductivity of the crystal, one has to characterize the heater lines first. The resistance R of the heater lines as a function of temperature, as well as temperature coefficient α and the heater length l are plotted in figure 2. All parameters are listed in table 1. The temperature-dependence shown in figure 2 of the resistance of metals is given by the Bloch-Grüneisen-relation [12] with the Debye-temperature for

Figure 2. Temperature-dependent resistance of the two metallic line heaters as well as the temperature coefficient α for one line heater. The measured resistance values are approximated with the Bloch-Grüneisen-relation [12] seen in equation (3). The heater parameters at room temperature are listed in table 1. These parameters of the heater lines are necessary to apply the 3ω-method.

Table 1. Heater parameters for the 2 heater lines used in this paper. l is the distance of the voltage contacts to measure $U_{1\omega}$ and $U_{3\omega}$ in 4-point geometry. R_0 and α_0 are specified for RT.

Sample	heater 1	heater 2
l	1.00 ± 0.5 mm	1.00 ± 0.5 mm
w	$20 \pm 1\ \mu$m	$40 \pm 1\ \mu$m
R_0	$17.30 \pm 0.04\ \Omega$	$8.97 \pm 0.02\ \Omega$
α_0	$0.002\,10 \pm 0.00002$ K^{-1}	$0.002\,13 \pm 0.00002$ K^{-1}

gold $\theta_D = 165$ K

$$R(T) - R(4.2\ \text{K}) \propto \left(\frac{T}{\theta_\text{D}}\right)^5 \int_0^{\theta_\text{D}/T} \frac{x^5}{(e^x - 1)(1 - e^{-x})} \mathrm{d}x. \tag{3}$$

4. Experimental results

To confirm the quality of the crystal and to determine the charge carrier part of the thermal conductivity a CZTS crystals electrical conductivity is measured as a function of temperature. The temperature-dependent electrical conductivity is shown in figure 3. It exhibits an increasing conductivity with increasing temperature. The measured conductivity values fit well with the assumption of Mott-variable-range-hopping following the equation

$$\sigma_\text{VRH} = \sigma_{0,\text{VRH}} T^{-1/2} \exp\left(-\frac{T_0}{T}\right)^{1/4}. \tag{4}$$

This correlation is shown linearized in figure 3(c)). A similar result was found by Nagaoka *et al* [13, 14] and Liu *et al* [6]. The strong occurrence of Mott-variable-range-hopping suggests a high amount of defects which act as occupied and unoccupied acceptor states forming an impurity band in the band gap. The kesterite crystal structure allows the formation of copper-zinc-antisides (Cu_{Zn}) and copper-vacancies (V_{Cu}) among others [15] which act as electrically active states. These impurities will have a non-neglectable influence on the thermal conductivity.

To determine the thermal conductivity one needs to measure $\Delta T (\ln(2\omega))$ first. Exemplary plots for three different temperatures are shown in figure 4. Besides $\Delta T(\omega)$, the 3ω-voltage $U_{3\omega}$ is plotted between 80 Hz and 1600 Hz. If ΔT is plotted against $\ln 2\omega$ a linear regime from 100 Hz to 1000 Hz is followed by a nonlinear regime for higher frequencies with a higher slope. The nonlinear slope belongs to the insulating photo resist which has a much lower thermal conductivity $\lambda_\text{PR} = 0.16 \pm 0.06$ Wm^{-1}K^{-1}. Therefore it dominates for high frequencies and low thermal penetration depths $\propto f^{-1/2}$ [11]. From the linear slope of the frequency spectrum we can examine the thermal conductivity of the sample using equation (2). Figure 5 shows the temperature-dependent thermal conductivity values. The displayed lines describing the phonon scattering are discussed below.
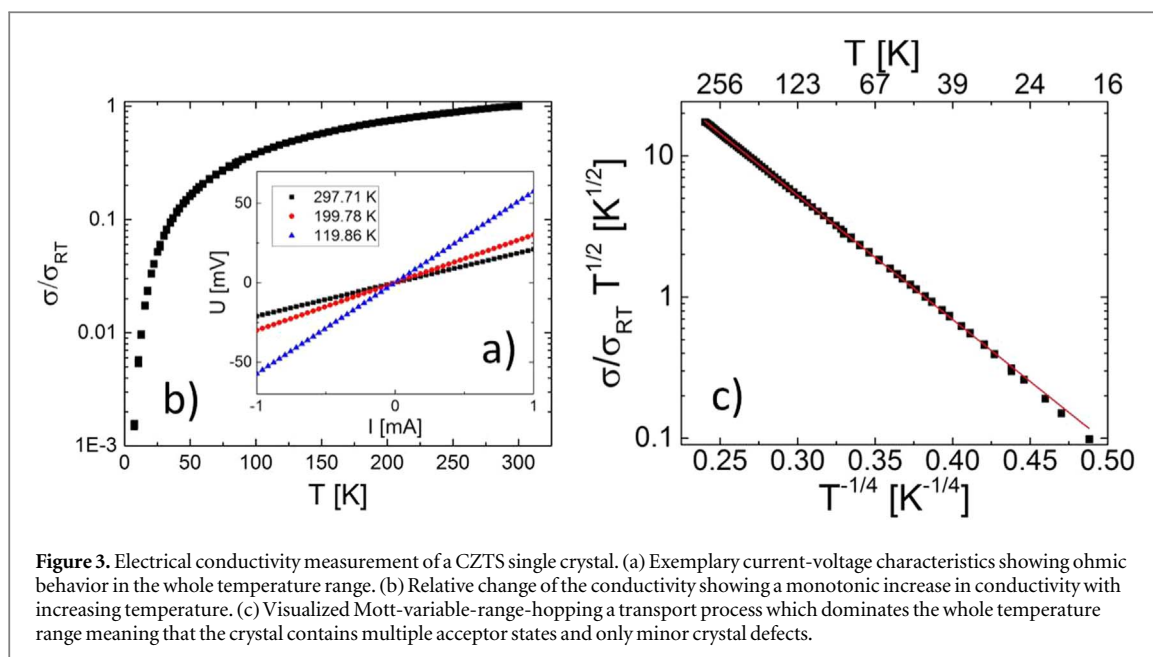
Figure 3. Electrical conductivity measurement of a CZTS single crystal. (a) Exemplary current-voltage characteristics showing ohmic behavior in the whole temperature range. (b) Relative change of the conductivity showing a monotonic increase in conductivity with increasing temperature. (c) Visualized Mott-variable-range-hopping a transport process which dominates the whole temperature range meaning that the crystal contains multiple acceptor states and only minor crystal defects.
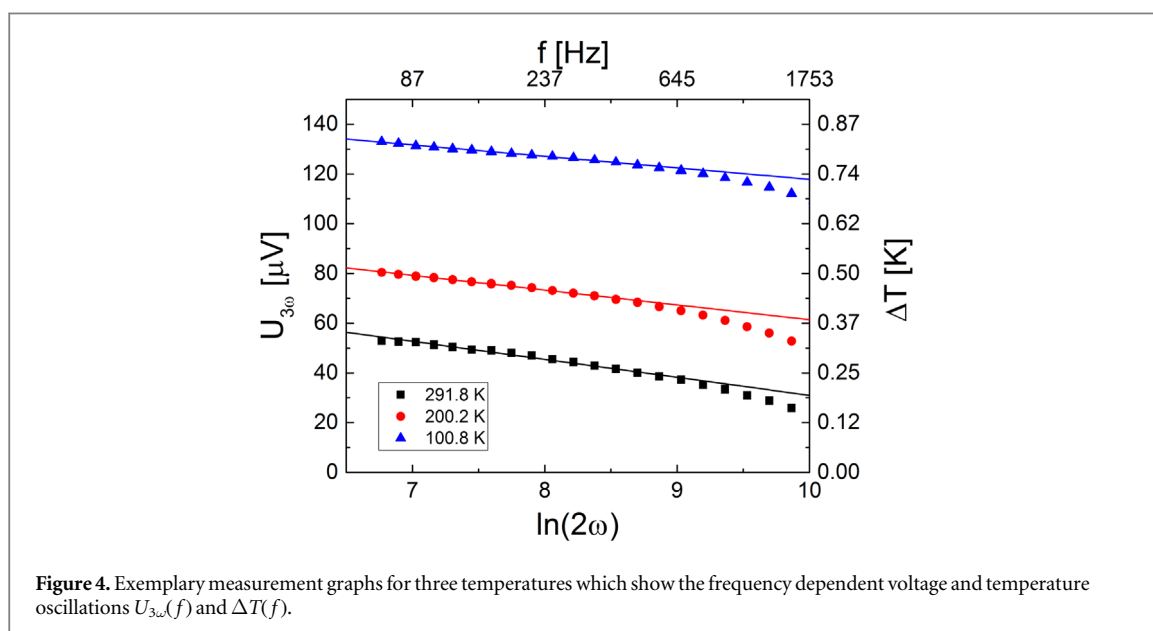

Figure 4. Exemplary measurement graphs for three temperatures which show the frequency dependent voltage and temperature oscillations $U_{3\omega}(f)$ and $\Delta T(f)$.

5. Discussion

The thermal conductivity at room temperature has a value of 5.1 ± 0.5 Wm^{-1}K^{-1}, measured with two different heater lines. As seen in figure 5 the thermal conductivity increases with decreasing temperature with a maximum at 100 K of 8.0 ± 0.5 Wm^{-1}K^{-1}. For temperatures below 100 K the thermal conductivity decreases monotonously with decreasing temperature. Unfortunately, the wider heater line 2 perished after the 175 K measurement point. The measured thermal conductivity is comparable to other published values listed in table 2. The deviation to other investigations is due to other growth processes. The best accordance of our values are with that of Liu *et al* [6] determined the Laser Flash Method from grown single crystals with values between 2.8 Wm^{-1}K^{-1} and 4.8 Wm^{-1}K^{-1} at room temperature. Further, they investigated the higher temperature range until 700 K and observed a decrease in the thermal conductivity with increasing temperatures, similar to our observations. Thompson *et al* [7] investigated polycrystalline thin CZTS films with the 3ω-method in a low temperature range and observed a maximum at 150 K which leads to an increase from room temperature 4 Wm^{-1}K^{-1} to 6.8 Wm^{-1}K^{-1} at low temperatures. Both values are below the single crystalline values and the maximum is at a higher temperature and might be related to higher defect scattering in polycrystalline material.

The thermal conductivity is usually a sum of the lattice thermal conductivity provided by phonons and the charge carrier thermal conductivity. The charge carrier thermal conductivity λ_{el} can be estimated by the
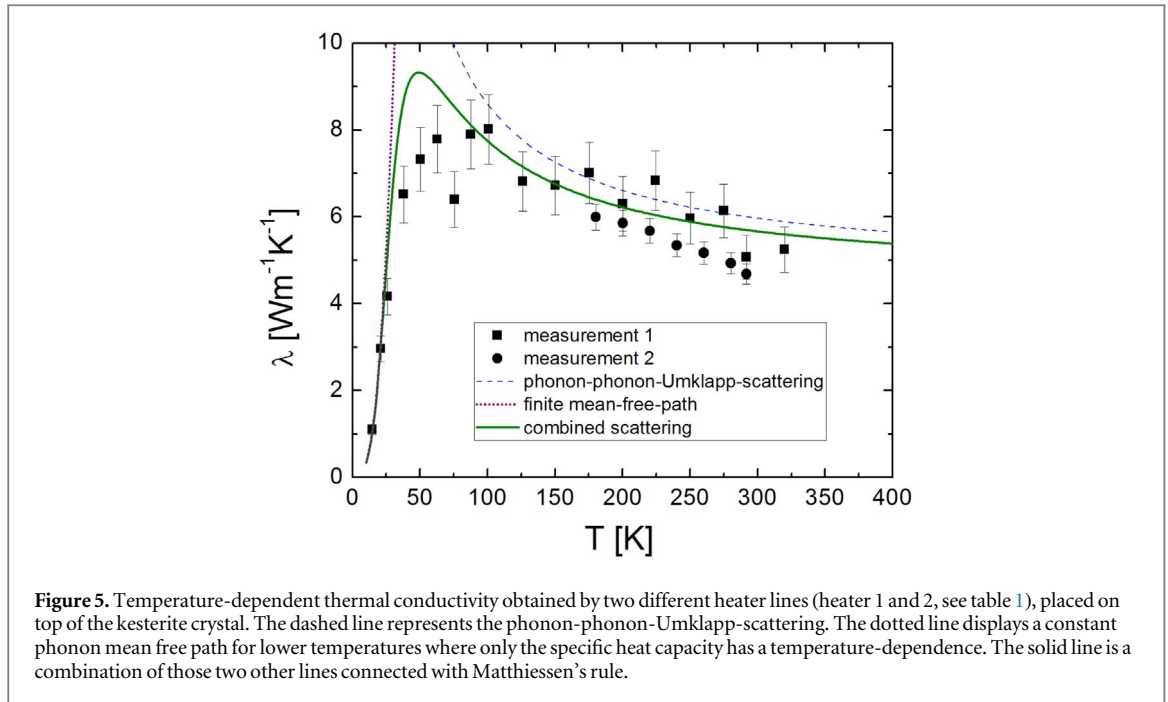
Figure 5. Temperature-dependent thermal conductivity obtained by two different heater lines (heater 1 and 2, see table 1), placed on top of the kesterite crystal. The dashed line represents the phonon-phonon-Umklapp-scattering. The dotted line displays a constant phonon mean free path for lower temperatures where only the specific heat capacity has a temperature-dependence. The solid line is a combination of those two other lines connected with Matthiessen's rule.

Table 2. Published thermal conductivity data for CZTS material at room temperature. Skelton *et al* [16] used DFT calculations to calculate the thermal conductivity values. Thompson *et al* [7] measured 1 μm thick polycrystalline films with the 3ω-method. Liu *et al* [6] measured crystals above room temperature and Yang *et al* [8] measured nanocrystals.

Source	Material	Thermal conductivity
This work	single crystal	5.1(0.5) $\mathrm{Wm^{-1}K^{-1}}$
Liu *et al* [6]	single crystal	4.8 $\mathrm{Wm^{-1}\,K^{-1}}$
Thompson *et al* [7]	polycrystal	4.0(2) $\mathrm{Wm^{-1}K^{-1}}$
Yang *et al* [8]	polycrystal	3 $\mathrm{Wm^{-1}K^{-1}}$
Skelton *et al* [16]	theory	2 $\mathrm{Wm^{-1}K^{-1}}$

Wiedemann–Franz-relation [17]

$$\lambda_{\mathrm{el}} = L\sigma T \quad \text{with} \quad L(T > \theta_{\mathrm{D}}) = 2.44 \ \mathrm{W\Omega K^{-2}}. \tag{5}$$
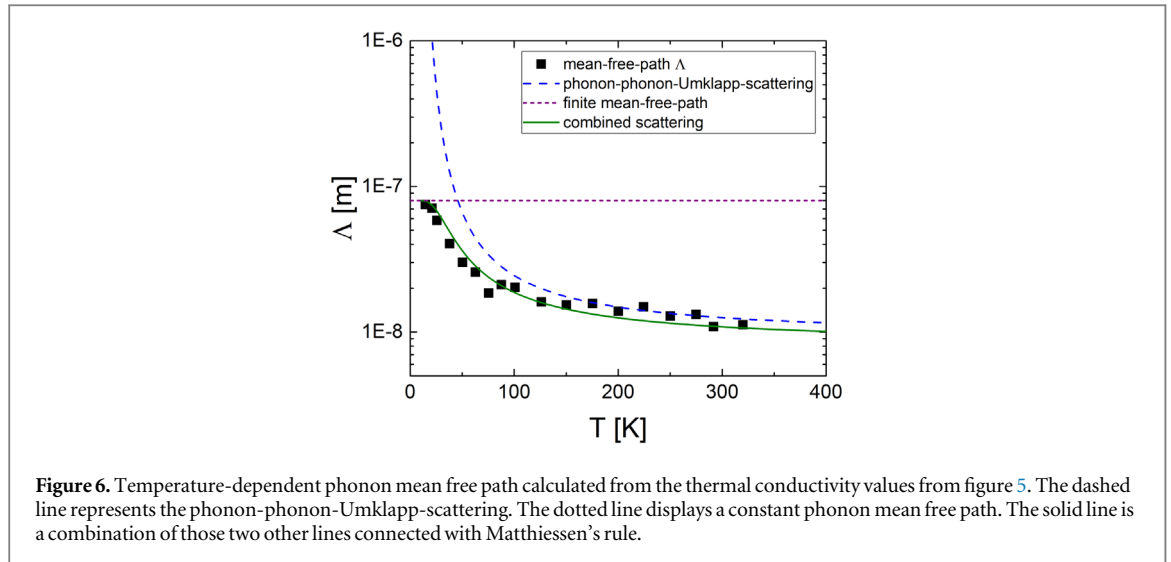
The Wiedemann–Franz-relation is valid only in the case of large angle scattering of charge carriers and phonons. Below the kesterite Debye temperature $\theta_{\mathrm{D}} = 302$ K [18] the Lorenz number L decreases due to the fact that the thermal resistance is determined by low angle scattering. But even then the Wiedemann–Franz-relation is suitable to determine the maximum charge carrier contribution to the thermal conductivity. Figure 3 shows the electrical conductivity of a single crystal, the expected Mott-variable-range hopping-conduction behavior

$$\sigma = \sigma_0 T^{-\frac{1}{2}} \exp\left(\frac{T}{T_0}\right)^{1/4} \tag{6}$$

and the calculated maximal charge carrier thermal conductivity $\lambda_{\mathrm{el}} = 7.3 \cdot 10^{-3} \ \mathrm{Wm^{-1}K^{-1}}$. This value is three orders of magnitude below the lattice thermal conductivity and will further decrease with decreasing temperature and therefore during the further procedure not considered.

The temperature-dependence of the lattice thermal conductivity λ can be explained with two different phonon-scattering models. The thermal conductivity is a product of the specific heat capacity C_V, the phonon mean free path Λ and the velocity of sound v_s

$$\lambda = \frac{1}{3}C_V\Lambda v_s. \tag{7}$$

Figure 6. Temperature-dependent phonon mean free path calculated from the thermal conductivity values from figure 5. The dashed line represents the phonon-phonon-Umklapp-scattering. The dotted line displays a constant phonon mean free path. The solid line is a combination of those two other lines connected with Matthiessen's rule.

The specific heat is given by [19]

$$C_V \propto \left(\frac{T}{\theta_D}\right)^3 \int_0^{\theta_D/T} \frac{x^4 e^x}{(e^x - 1)^2} dx \tag{8}$$

and the mean free path in case of phonon-phonon-Umklapp scattering is given by

$$\Lambda_{ph-ph} \propto (e^{\theta_D/2T} - 1). \tag{9}$$

In the case of additional independent scattering mechanisms one has to combine them with Matthiessen's Rule [20]

$$\frac{1}{\Lambda} = \frac{1}{\Lambda_{ph-ph}} + \frac{1}{\Lambda_{imp}}. \tag{10}$$

Due to the exponential increase of Λ_{ph-ph} at low temperature, the phonon mean free path is determined by Λ_{imp}. We assume a constant mean free path value for the scattering term Λ_{imp} to approximate the experimental data. As seen in figure 5 this assumption can be used to get the best accordance of the approximation aligned at low and high temperatures for Λ_{ph-ph} and Λ_{imp} respectively. The calculated mean free path values are shown in figure 6. In figure 6 it can be seen that the highest calculated mean free path value is still below 100 nm and therefore below the crystal height which is several hundred microns. The boundary for the phonons is not the crystal itself but impurities. The best fitting result are achieved with the constant mean free path value of $\Lambda_{imp} = 80$ nm. Assuming this value is given by impurities the lower limit of the impurity density is $n_{imp} = 2 \cdot 10^{15}$ cm^{-3} and the lower limit of their concentration would be $c_{imp} = 0.2$ ppm. Since hopping is the main conduction mechanism and keserites have at least six different impurity types [15] even a higher concentration is expected.

6. Conclusion

A thermal conductivity for kesterite CZTS single crystals at room temperature was measured to be 5.1 Wm^{-1}K^{-1} and a maximal thermal conductivity of 8.0 Wm^{-1}K^{-1} was found at 100 K. We conclude that acceptor states in the CZTS material leads to a domination of Mott-variable-range-hopping for the electrical conductivity and a maximum for the thermal conductivity at 100 K due to phonon-impurity-scattering. Our measurement give an upper limit for the thermal conductivity. The values will be reduced for applications of polycrystalline films for solar devices due to additional phonon-grain-boundary-scattering processes.

Acknowledgments

ORCID iDs

M Handwerg ⓘ https://orcid.org/0000-0003-1235-9996
S Schorr ⓘ https://orcid.org/0000-0002-6687-614X

References

[1] Green M A, Emery K, Hishikawa Y, Warta W and Dunlop E D 2015 *Prog. Photovoltaics Res. Appl.* **23** 805
[2] Schorr S 2011 *Sol. Energy Mater* **95** 1482
[3] Schorr S, Gurieva G, Guc M, Dimitievska M, Perez-Rodriguez A, Izquierdo-Roca V, Schnohr C, Kim J, Jo W and Merino J M 2020 *J. Phys. Energy* **2** 012002
[4] Shockley W and Queisser H J 1961 *J. Appl. Phys.* **32** 510
[5] Wang W, Winkler M T, Gunawan O, Gokmen T, Todorov T K, Zhu Y and Mitzi D B 2014 *Adv. Energy Mater* **4** 1301465
[6] Liu M-L, Huang F-Q, Chen L-D and Chen I-W 2009 *Appl. Phys. Lett.* **94** 202103
[7] Thompson W D, Nandur A Jr. and White B E Jr. 2016 *J. Appl. Phys.* **119** 095108
[8] Yang H, Jauregui L A, Zhang G, Chen Y P and Wu Y 2012 *Nano Lett.* **12** 540
[9] Levcenco S, Dumcenco D, Wang Y P, Huang Y S, Ho C H, Arushanov E, Tezlevan V and Tiong K K 2012 *Opt. Mater.* **34** 1362
[10] Dumcenco D and Huang Y S 2013 *Opt. Mater.* **35** 419
[11] Cahill D G 1990 *Rev. Sci. Instrum.* **61** 802–8
[12] Bloch F 1928 *Z. Phys.* **52** 555
[13] Nagaoka A, Miyake H, Taniyama T, Kakimoto K and Yoshino K 2013 *Appl. Phys. Lett.* **103** 112107
[14] Nagaoka A, Katsube R, Nakatsuka S, Yoshino K, Taniyama T, Miyake H, Kakimoto K, Scarpulla M A and Nose Y 2015 *J. Crys. Growth* **423** 9
[15] Rios L E V, Neldner K, Gurieva G and Schorr S 2016 *J. Alloy. Comp.* **657** 408
[16] Skelton J M, Jackson A J, Dimitrievska M, Wallace S K and Walsh A 2015 *APL Mater* **3** 041102
[17] Wiedemann G and Franz R 1853 *Ann. Phys.* **89** 497
[18] Adachi S 2015 *Earth-Abundant Materials for Solar Cells: Cu2IIIVVI4 Semiconductors* **1** 364
[19] Tritt T M 2004 *Thermal Conductivity Theory, Properties, and Applications* **1** 94
[20] Matthiessen A 1862 *Rep. Br. Assoc.* **32** 144